

Improving fire severity prediction in south-eastern Australia using vegetation specific information

Kang He^{1,2}, Xinyi Shen³, Cory Merow^{2,4}, Efthymios Nikolopoulos⁵, Rachael V. Gallagher⁶, Feifei Yang^{1,2}, Emmanouil N. Anagnostou^{1,2}

¹Department of Civil and Environmental Engineering, University of Connecticut, Storrs, CT 06269, USA

²Eversource Energy Center, University of Connecticut, Storrs, CT 06269, USA

³School of Freshwater Sciences, University of Wisconsin, Milwaukee, Milwaukee, WI, 53204, USA

⁴Department of Ecology and Evolutionary Biology, University of Connecticut, Storrs, CT 06269, USA

⁵Department of Civil and Environmental Engineering, Rutgers University, Piscataway, NJ 08854, USA

⁶Department of Biological Sciences, Macquarie University, North Ryde, NSW 2109, Australia

Correspondence to: Emmanouil N. Anagnostou (emmanouil.anagnostou@uconn.edu)

Abstract. Wildfire is a critical ecological disturbance in terrestrial ecosystems. Australia, in particular, has experienced increasingly large and severe wildfires over the past two decades while globally fire risk is expected to increase significantly due to the projected increase in extreme weather and drought condition. Therefore, understanding and predicting fire severity is critical for evaluating current and future impacts of wildfires on ecosystems. Here, we firstly introduce a vegetation-type specific fire severity classification applied on satellite imagery, which is further used to predict fire severity using antecedent drought conditions, fire weather (i.e., wind speed, air temperature and atmospheric humidity), and topography of the fire season (November to March). Compared with fire severity maps from Fire Extent and Severity Mapping (FESM) dataset, we find fire severity prediction results using the vegetation-type specific thresholds show good performance in extreme and high severity classification with accuracy of 0.64 and 0.76, respectively. Based on a ‘leave-one-out’ cross-validation experiment, we demonstrate high accuracy for both the fire severity classification and the regression using a suite of performance metrics: determination coefficient (R^2), mean absolute error (MPE) and root mean square error (RMSE), which are 0.89, 0.05, and 0.07, respectively. Our results also show that the fire severity prediction results using the vegetation-type specific thresholds could better capture the spatial patterns of fire severity, and has the potential to be applicable for seasonal fire severity forecast due to the availability of seasonal forecasts of the predictor variables.

Keywords: Fire severity; Normalized Burning Ratio; Random Forest; Vegetation type; Severity classification.

1 Introduction

Fire is recognized as a critical disturbance in ecosystems, which shapes vegetation across several continents (Archibald et al., 2013; Gill, 1975; Giglio et al., 2010; Gomez et al., 2015). In recent decades, wildfires have affected extensive areas in forests and woodlands across the globe, including those in Australia where over 10 million hectares were burned in the 2019-2020 fire season (from November to March, Gallagher et al. 2021). These fires are considered unprecedented in contemporary Australian fire history (Nolan et al., 2020; Shine, 2020), and more severe fires are expected in the future due to the impacts of

33 climate change on fire-weather and dynamics (Hennessy et al., 2005). Changes in fire conditions are also anticipated globally
34 (Abatzoglou et al. 2019). Therefore, predicting fire characteristics – such as severity – will be essential for evaluating current
35 and future impact of wildfires on ecosystems worldwide.

36 Fire severity, defined here as the magnitude of change in vegetation associated with fire, is routinely used to describe the
37 impact of wildfires on vegetation, soil and wildlife (Lentile et al. 2006; Keeley 2009). Field survey and remote sensing-based
38 evaluations of burn severity are commonly used by fire scientists and managers. Field survey-based evaluations involve
39 assessing the amount of biomass consumed (Keeley, 2009), measuring the changes in vegetation height (Wang and Glenn,
40 2009) or surface fuel consumption (Boby et al., 2010; Hudak et al., 2013). By contrast, remotely sensed evaluations of burn
41 severity use satellite imagery to quantify the magnitude of vegetation changes between pre-fire and post-fire conditions, in
42 terms of the changes in surface reflectance (Holden et al., 2009; Miller et al., 2009; Soverel et al., 2010) (e.g. the difference
43 between pre- and post-fire Normalized Burn Ratio (dNBR), Keeley, 2009).

44 Statistical approaches, which incorporate factors such as topography, weather and water availability provide insight into
45 possible drivers of fire severity (Morgan et al., 2014). For instance, Bradstock et al. (2010) investigated the effects of weather,
46 fuel and terrain on fire severity in south-eastern Australia. They found weather was the predominant influence on fire severity
47 while the influence of terrain was stronger under moderate conditions. Similarly, a study by Collins et al. (2013) examined the
48 relationships between environmental variables (i.e., fire weather, topography and fuel age) and fire severity in south-eastern
49 Australia and whether it can be modified by increasing mean annual precipitation. They concluded that the relationships
50 between crown fire and weather, topography and fuel age were largely unaltered across the precipitation gradient. Collins et
51 al. (2019) also examined the relative effect of fire weather, drought severity and landscape features (i.e., topography, fuel age,
52 vegetation type) on the occurrence of fire refugia in south-eastern Australia. They found that the fire weather and drought
53 severity were the primary drivers of the occurrence of fire refugia, moderating the effect of landscape attributes. Furthermore,
54 Clarke et al. (2014) investigated fire severity control factors, including landscape/vegetation or weather, providing evidence
55 that even though strong weather controls, fire history, terrain and vegetation shape the immediate effect. In addition, Bowman
56 et al. (2021) demonstrated that overwhelming dominance of fire weather in driving complete scorch or consumption of forest
57 canopies in natural and plantation forests in the 2019-20 megafires.

58 Despite the emerging evidence that statistical modelling with multiple biophysical and environmental predictor variables can
59 provide high accuracy estimates of fire severity, this technique is not widely adopted in major areas of known fire risk. One
60 such region is the southeast coast of Australia which is subject to annual fire seasons (from November to March, Collins et al.,
61 2022) vary in extent and severity and has a high richness of endemic plant species adapted to particular fire regimes (Gallagher
62 et al., 2021). Besides, an accurate representation of fire severity levels is important for managing and mitigating the effects of
63 wildfires, both in terms of emergency response and long-term ecological recovery. Existing fire severity classification schemes
64 rely on the in-situ measurements of Composite Burn Index (CBI, Key and Benson, 2006; Lutes et al., 2006) and/or aerial
65 photographs identification (Collins et al., 2018; Dixon et al., 2022) which are available for certain regions and for limited
66 vegetation types under certain climate (Eidenshink et al., 2007; Keeley et al., 2009; Tran et al., 2018). However, obtaining

67 CBI and interpreting aerial photographs are labor-intensive and time-consuming, especially over large areas, while inferring
68 fire severity levels directly from satellite-derived dNBR can be more efficient for large-scale applications, yet no dNBR-based
69 fire severity classification scheme exists for regions such as the southeast coast of Australia, which is subject to recurring
70 annual wildfires and varies greatly in vegetation types with high richness of endemic plant species adapted to particular fire
71 regimes (Gallagher et al., 2021).

72 Understanding current and predicting future fire severity in eastern Australia is critical for evaluating the potential for increased
73 extinction risk due to recurrent high severity fires (Enright et al. 2015) and is important for supporting ecologically informed
74 fire management (Clarke et al. 2019). Therefore, the predictor variables involved in the fire severity model should be accessible
75 for both historical events and projected future events (e.g. seasonal, climate).

76 In this study, we newly propose a vegetation specific fire severity classification scheme for predicting fire severity and
77 demonstrate its performance across the Australian state of New South Wales (NSW). Using drought conditions, vegetation
78 type, and fire weather conditions during the fire season as input, our modelling approach applies the Random Forest (RF)
79 classification method to predict the dNBR – an indicator of burn severity derived from Landsat imagery. We demonstrate
80 model performance based on 20 years of wildfire data from NSW through a leave-one-year-out cross-validation experiment.

81 **2 Study area**

82 New South Wales (NSW) in south-eastern Australia (Figure 1) occupies a subtropical-temperate climate region with relatively
83 mild weather and distinctive seasons (e.g., hot summers and cold winters) (Speer et al., 2009). Mean annual and extreme
84 temperatures are highest in the northwest of the state whereas average maximum temperatures in coastal areas range from
85 26 °C to 16 °C, while the average minimum temperature falls between 19 ° and 7 °C. There is a strong precipitation gradient
86 from east to west across the state, with annual precipitation on the eastern coast ranging between 600 mm/year and 1200
87 mm/year decreasing to generally less than 180 mm/year in the north west of the state
88 Vegetation across the study region is predominantly wet and dry sclerophyll forests, although is interspersed with areas of
89 rainforest, woodlands and coastal heath (Keith 2004).

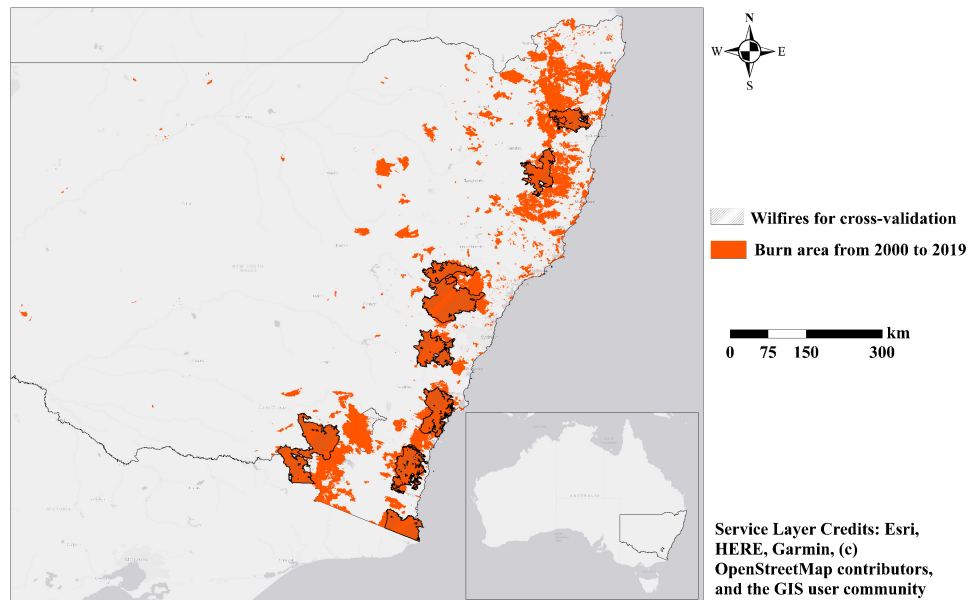


Figure 1. Locations of study wildfires over New South Wales (NSW), Australia. The burn area is from NSW National Parks and Wildlife Service (NPWS) Fire History – Wildfire and Prescribed Burns dataset.

90 **3 Data and method**

91 **3.1 Model Input and output**

92 **3.1.1 Fire extent**

93 The spatial extent of annual fires between 2000 to 2019 is accessed from the NSW National Parks and Wildlife Service (NPWS)
 94 Fire History – Wildfire and Prescribed Burns dataset ([https://datasets.seed.nsw.gov.au/dataset/fire-history-wildfires-and-](https://datasets.seed.nsw.gov.au/dataset/fire-history-wildfires-and-prescribed-burns-1e8b6)
 95 [prescribed-burns-1e8b6](https://datasets.seed.nsw.gov.au/dataset/fire-history-wildfires-and-prescribed-burns-1e8b6)), produced by the Department of Planning, Industry and Environment. The NPWS Fire History is a
 96 spatial polygon layer, with each polygon recording the boundary, start date, end date, and burn area. We use the NPWS
 97 polygons whose burn areas are greater than 1 km² as the mask to include only the fire impacted areas. While this dataset is
 98 unlikely to be a complete record of all fire events, it represents the largest single repository of fire extent data in NSW.

99 **3.1.2 Fire severity**

100 As a widely used fire severity index, the dNBR is calculated by subtracting the post-fire NBR raster from the pre-fire NBR
 101 raster as in Eq (1) (Keeley, 2009):

102
$$dNBR = PrefireNBR - PostfireNBR \quad (1)$$

103 The formula of NBR is similar to the normalized difference vegetation index (NDVI), except that it uses near-infrared (NIR)
 104 and shortwave-infrared (SWIR) bands, as written in Eq (2) (García and Caselles, 1991; Key and Benson, 2006). NBR can be

105 computed by the Thematic Mapper (TM) and Enhanced Thematic Mapper Plus (ETM+) sensors on using Band 7 as the short-
106 wave infrared (SWIR) and Band 4 for Landsat 4-7 and Band 5 for Landsat 8 as the near infrared (NIR) reflectance, respectively.
107 While in Sentinel-2, SWIR and NIR are represented by Band 8 and Band 12, respectively.

$$108 \quad NBR = \frac{NIR - SWIR}{NIR + SWIR} \quad (2)$$

109 We calculate the dNBR within the fire boundaries from Landsat and Sentinel archive imagery, using the start date and end
110 date to determine the pre-fire and post-fire dates. In this study, the pre-fire NBR (preNBR), is used as a proxy of the initial
111 condition of vegetation. The calculation of a dNBR-image is described as follows: (1) determine a individual fire from NPWS
112 Fire History; (2) collect the most recent Landsat images based on the tags demarcating the start and end times of each individual
113 fire; (3) apply a cloud- and snow-masking algorithm to remove snow, clouds, and their shadows from all imagery based on
114 each sensor's pixel quality assessment band; (4) use the auxiliary satellite images (e.g., Sentinel-2) to fill the blank pixels in
115 the cloud-free images from step (3) to obtain the pre and post NBR composites; (5) subtract pre- and post-NBR images to
116 create a dNBR composite with the smallest possible cloud and shadow extent. The dNBR typically ranges from -2 to +2, with
117 high positive values indicating severe burn damage where the vegetation has been completely consumed. Values around zero
118 suggest either unburned areas or areas where the fire had a very low impact. Negative values can indicate an increase in
119 vegetation, which might be due to vegetation recovery over time or errors in the analysis.

120 **3.1.3 Vegetation**

121 Vegetation composition and structure are expected to influence fire propagation and severity (Collins et al., 2007) and the
122 vegetation type is also used as a proxy for vegetation structure (Hammill et al., 2006). The dominant vegetation over NSW is
123 wet and dry sclerophyll forests (Keith 2004). Wet sclerophyll forests can be divided into two subgroups (the shrubby sub-
124 formation and the grassy sub-formation), which have a tall canopies dominated by Eucalyptus and a monophyllous understory
125 ([https://www.environment.nsw.gov.au/threatenedSpeciesApp/VegFormation.aspx?formationName=Wet+sclerophyll+forests
126 +\(grassy+sub-formation\)](https://www.environment.nsw.gov.au/threatenedSpeciesApp/VegFormation.aspx?formationName=Wet+sclerophyll+forests+(grassy+sub-formation))). Two sub-formations of dry sclerophyll forests also occur: shrub/grass and shrubby. This study
127 focuses on burn severity for the dominant sclerophyll forests (Figure 1). The vegetation map is intersected with NPWS
128 polygons to identify the areas where sclerophyll forests have previously burned.

129 **3.1.3 Topography**

130 Prior studies report strong control of topography on burn severity, by influencing fire behavior, fuel moisture, and water
131 balances (Fang et al., 2018, Harris and Taylor, 2015, Holden et al., 2009). Therefore, we include three topographic measures
132 from Shuttle Radar Topography (SRTM, <https://www2.jpl.nasa.gov/srtm/world.htm>), elevation (DEM), slope (Slope), and
133 Topographic Position Index (TPI). TPI helps in identifying landform features such as ridges, valleys, slopes, and plateaus
134 (Weiss, 2001). Positive TPI values indicate locations that are higher than the average of their surroundings (e.g., hilltops or

135 ridges), while negative TPI values indicate locations that are lower than their surroundings (e.g., valleys or depressions). Values
136 close to zero may represent flat areas or slopes.

137

138 **3.1.3 Weather**

139 In addition to fuels and terrain, weather is another important factor in wildfires. The McArthur Forest Fire Danger Index (FFDI,
140 McArthur 1967) is an empirical relationship comprising the short-term meteorological conditions and the long-term drought
141 factor (Dowdy et al. 2009). The FFDI is currently used operationally by the Australian Bureau of Meteorology (BoM) to
142 produce fire weather warnings to authorities, which is defined as:

$$143 \quad FFDI = 2 \times e^{(-0.45+0.897 \ln DF - 0.0345 RH + 0.038 T + 0.0234 V)} \quad (3)$$

144 where DF is the drought factor; and RH, T and V represent the relative humidity, surface air temperature and wind velocity,
145 respectively. In this study, we extract daily temperature, relative humidity and wind speed data from the ERA5-Land global
146 dataset over the burn areas (<https://cds.climate.copernicus.eu/cdsapp#!/dataset/reanalysis-era5-land?tab=form>).

147 The DF is estimated using the Keetch–Byram Drought Index (KBDI, Keetch and Byram 1968). KBDI is a continuous reference
148 scale describing the dryness of the soil and duff layers. The index increases for each day without rain and decreases when it
149 rains. KBDI is world widely used for drought monitoring for national weather forecast, wildfire prevention. KBDI over burnt
150 areas can be accessed in Takeuchi et al. (2015). The daily FFDI and KBDI values for the day prior to the start of the wildfires
151 are used as the predictors in predicting burn severity, owing to the strong correlation in time between extreme values of the
152 FFDI and the start of the wildfires [Dowdy et al., 2009] Using the most potential extreme FFDI, indicating the extreme weather
153 conditions, in the period leading up to a wildfire could address the impact of weather on wildfire risk.

154 **3.2 Method**

155 We newly propose an alternative way to determine the optimal thresholds in fire severity classification for different vegetation
156 types. The dNBR of all burnt pixels for each vegetation type are collected and a set of dNBR values at the quantiles varying
157 from 5% to 35% representing the threshold for low severity classification, quantiles varying from 35% to 65% representing
158 the threshold for moderate severity classification, and quantiles varying from 65% to 95% representing the threshold for high
159 severity classification. For example, a classified burn severity sample can be obtained using the thresholds for high, moderate,
160 and low severity at 85% quantile, 55% quantile and 25% quantile, respectively. Secondly, a fire severity prediction model is
161 developed for each severity category based on the fire severity classification results, to provide the numeric prediction of
162 dNBR.

163 **3.2.1 Fire severity classification by RF**

164 Random Forest is developed as an extension of the classification and regression tree (CART) to improve the accuracy and
165 stability of the CART model (Breiman 2001). The steps of the RF algorithm are briefly summarized as: (i) randomly generate

166 *n*tree bootstrap samples of the original data. The elements not selected are referred to as ‘out of bag’ (OOB) samples. (ii) for
167 each split, randomly select *m_{try}* predictors of the original predictors and choose the best predictor among the *m_{try}* predictors
168 to partition the data. (iii) predict new data (OOB elements) by averaging predictions of the *n*tree trees; and (iv) the OOB
169 samples are used to estimate the prediction error. The RF can also provide a measurement of variable importance. One of the
170 approaches is to look at the increase in the OOB estimate error when the specific predictor variable is randomly permuted and
171 other predictors are constant. The more the error increases, the more important the variable is. These variable importance
172 values are used to rank the predictors in terms of their relative contribution to the model. The RF model was generated using
173 the package randomforest in R (<https://cran.r-project.org/web/packages/randomForest/>).

174

175 **3.2.2 Fire severity prediction by XGboost**

176 For the regression model, we implement the Extreme Gradient Boosting (XGBoost) algorithm, one of the most popular
177 supervised machine learning algorithms proposed by Chen et al. (2015). XGBoost employs a gradient boosting framework
178 that iteratively trains a sequence of weak prediction models and combines them into a strong model. In addition to gradient
179 boosting, XGBoost implements several advanced features, including regularization techniques to prevent overfitting, parallel
180 processing to speed up training, and built-in support for missing data (Chen and Guestrin, 2016). In the XGBoost algorithm,
181 complex interactions are modeled, and other complexities such as missing values in the predictors are managed without almost
182 any loss of information. Selection of features is performed by a combination of parameters (e.g., number of iterations, learning
183 rate) and the unique combinations of each attribute in the training data set. The XGBoost model is generated using the package
184 xgboost in R (<https://cran.r-project.org/web/packages/xgboost/>).

185

186 **3.2.3 Calibration and validation**

187 The fire severity classification maps from Fire Extent and Severity Mapping (FESM,
188 <https://datasets.seed.nsw.gov.au/dataset/fire-extent-and-severity-mapping-fesm>) in period from 2016 to 2019 are used as the
189 independent source to validate the fire severity classification results based on the proposed method. To evaluate the model’s
190 performance, we also use “leave -one group-out” for training and validation. The fire samples from 2000 to 2019 are firstly
191 divided into 20 subsets depending on the year the fire occurred, and this holdout method is repeated 20 times. Each subset
192 represents the samples from the wildfire with the largest burn area in the corresponding year. Secondly, at each time, one of
193 the 20 subsets is used as the testing set, and the remaining 19 subsets are put together to form the training set. Thirdly, the
194 average error across all 20 trials is computed. The advantage of this cross-validation method is that it gives us an indication of
195 how well the model would do when making new predictions for data it has not already seen.

196 For performance evaluation of multiclass event classification, accuracy is expressed as the proportion of correctly predicted
197 events over all predicted events, which is calculated as Eq (4):

198
$$Accuracy = \frac{Number\ of\ correct\ predictions}{Number\ of\ all\ predictions} \quad (4)$$

199 While precision is expressed as the proportion of events correctly predicted as label X (low, moderate, or high) over all events
200 predicted as label X (Eq (5)).

201
$$Precision = \frac{True\ Positive}{True\ Positive + False\ Positive} \quad (5)$$

202 in which True Positive represents the situation both observation and prediction are labelled as X, False Positive represents
203 observation is not labelled as X but prediction as label X.

204 Recall is calculated as:

205
$$Recall = \frac{True\ Positive}{True\ Positive + False\ Negative} \quad (6)$$

206 in which False Negative represents the situation observation is label X but prediction is not label X.

207 Combining metrics of Precision and Recall, the F1 Score is the harmonic mean of Precision and Recall. The F1 Score gives
208 equal weight to Precision and Recall. A maximized F1 Score could create a balanced classification model, and is calculated as
209 follows:

210
$$F1\ score = 2 * \frac{Precision * Recall}{Precision + Recall} \quad (7)$$

211

212 The coefficient of determination (R^2) is used to measure how well the prediction agreed with the actual values. The formula
213 of R^2 is described as:

214
$$R^2 = \frac{1}{n} \sum_{i=1}^n \frac{(o_i - \frac{\sum_{i=1}^n o_i}{n})(p_i - \frac{\sum_{i=1}^n p_i}{n})^2}{o_i p_i} \quad (8)$$

215 Where o_i and p_i represent the actual and predicted values for sample i ; n is the total number of samples. The higher R^2
216 indicates better fit of the model predictions to the actual values with best value of 1.

217 The mean absolute error (MAE) the mean relative error, the lower MAE is, the better the model performed.

218
$$MAE = \frac{\sum_{i=1}^n |p_i - o_i|}{n} \quad (9)$$

219 The root mean square error (RMSE) is used to quantify the random component of the error. The lower RMSE indicates better
220 model performance.

221
$$RMSE = \sqrt{\frac{\sum_{i=1}^n (p_i - o_i)^2}{n}} \quad (10)$$

222

223 **4 Results**

224 **4.1 Fire severity of burnt vegetation**

225 Over the past 20 years, wildfire history databases managed by government agencies indicate that approximately 112,590 km²
226 have been recorded as affected by fires in NSW, of which, almost 53,830 km² burned during the 2019-20 megafires (Figure
227 2). This dataset indicates that the annual burn area is typically below 5,000 km², but in exceptional years such as 2002 and
228 2003, the affected area can reach more than 10,000 km². The affected area from the 2019-20 fires is approximately 10 times
229 larger than those in other years from 2004 to 2018.

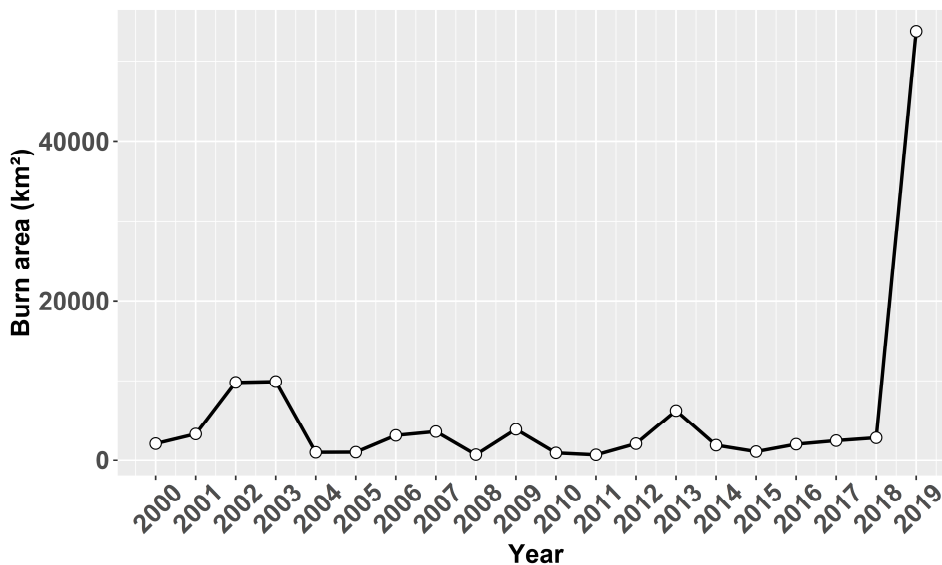
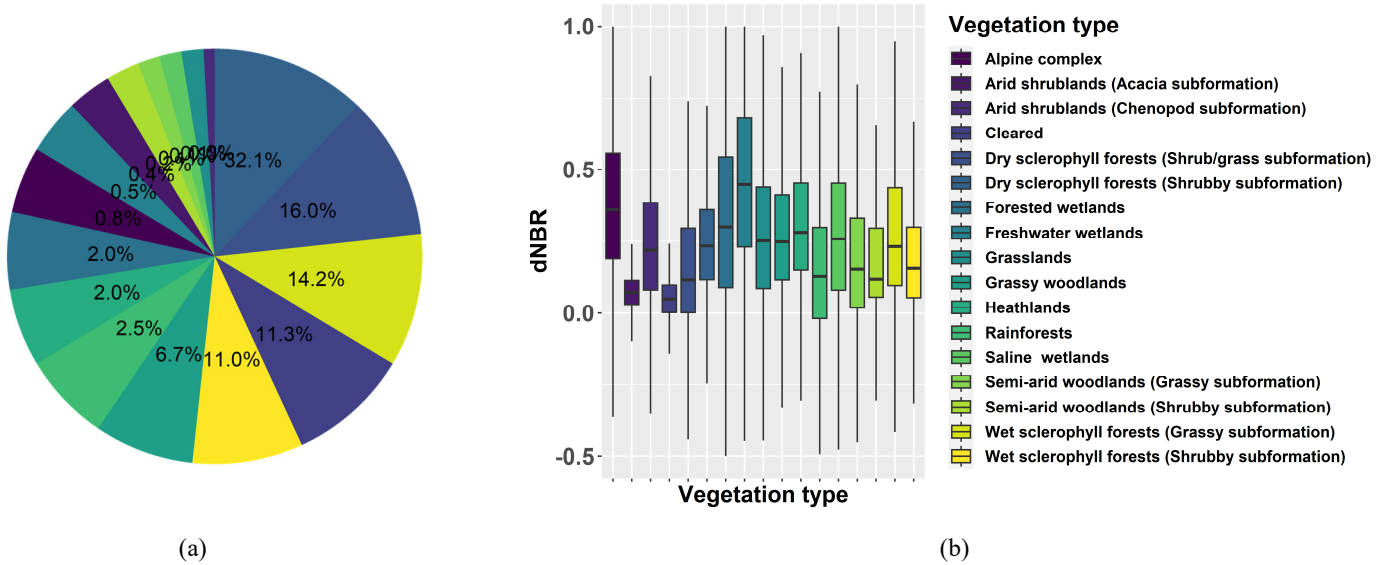


Figure 2. Annual burnt area (km²) across New South Wales, in south-eastern Australia.

230 Among the burnt area, the fractions of vegetation types are shown in Figure 3 (a). The dry sclerophyll forests (shrubby
231 subformation) accounted for the largest proportion of the burnt area (32.1%), followed by the dry sclerophyll forests
232 (shrub/grass subformation) which account for 16%. The wet sclerophyll forests (grassy subformation) occupy 14.2% of the
233 burnt area, while for the wet sclerophyll forests (shrubby subformation) the proportion is 11%. Specifically, the cleared area
234 accounted for 11.3% of the burnt area, approximately equal to those of the wet sclerophyll forests (shrubby subformation).
235 Other vegetation types largely affected by the wildfires are grassy woodlands, rainforest and heathlands, the proportion of
236 which are 6.7%, 2.5% and 2%, respectively. The distribution of fire severity indicated by dNBR for each vegetation type is
237 displayed as Figure 3 (b). These boxplots in Figure 3 (b) show that the fire severity varies significantly with vegetation type,
238 demonstrating that the vegetation specific thresholds should be applied in fire severity classification. For example, the fire
239 severity of cleared areas is overall the smallest while the fire severity of heathland shows the overall largest. The fire severity

240 varies even for the major vegetation type with different subgroups, for instance, the fire severity of dry sclerophyll forests with
 241 shrubby subformation is larger than the fire severity of dry sclerophyll forests with shrub/grass subformation.
 242

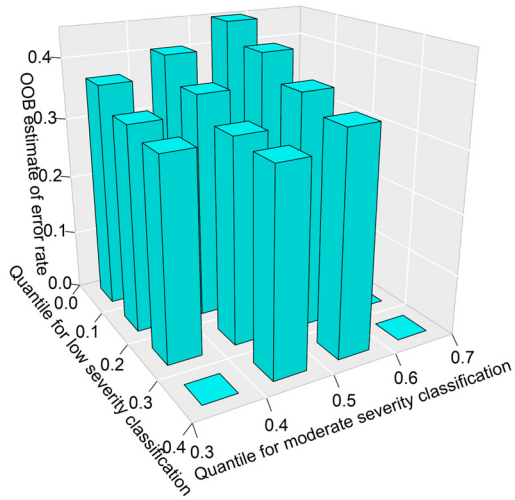


243 Figure 3. (a) The proportion of burnt area and (b) the distribution of fire severity grouped by vegetation type, over NSW from 2000 to 2019

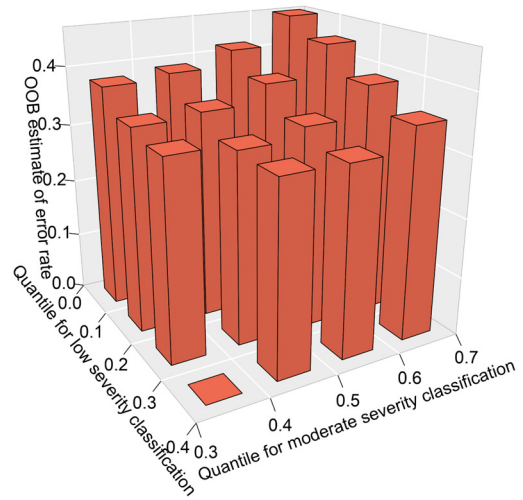
244 **4.2 Threshold determination for fire severity classification**

245 Given the variability shown in Figure 3 (b), we proposed an alternative way to determine the optimal thresholds in fire severity
 246 classification for different vegetation types. To determine these thresholds the dNBR of all burnt pixels for the vegetation type
 247 were collected and a set of dNBR values at the quantiles from 0.05 to 0.95 are used as the candidates of thresholds for the fire
 248 severity classification. The classified samples using the threshold of dNBR at the quantiles are imported as the training set in
 249 RF models and the OOB estimate of error rate is recorded for the training samples. Figure 4 (a), (b), (c) and (d) show the
 250 variations of OOB estimate of error rate changes with thresholds of dNBR at the quantiles varying from 5% to 35% (low
 251 severity threshold)/35% to 65% (moderate severity threshold), when the high severity threshold are set as the dNBR values at
 252 the 65%, 75%, 85% and 95% quantiles, respectively. The optimal thresholds are determined when the lowest OOB estimate
 253 of error rate is found. For example, for dry sclerophyll forests (shrubby subformation), the thresholds for high, moderate and
 254 low severity classification are 0.55 (85% quantile), 0.38 (55%) and 0.20 (25%), respectively. It is important to be aware that
 255 the classification step is merely used to improve the consecutive regression accuracy, rather than the final severity
 256 categorization result. The choice of threshold in this step therefore will not affect severity categorization. The categorization
 257 will be solely based on predicted severity value, using user defined thresholds.

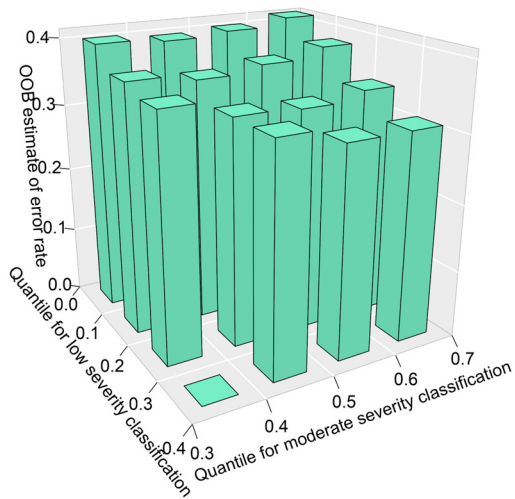
OOB estimate of error rate at 0.65 quantile for high severity classification



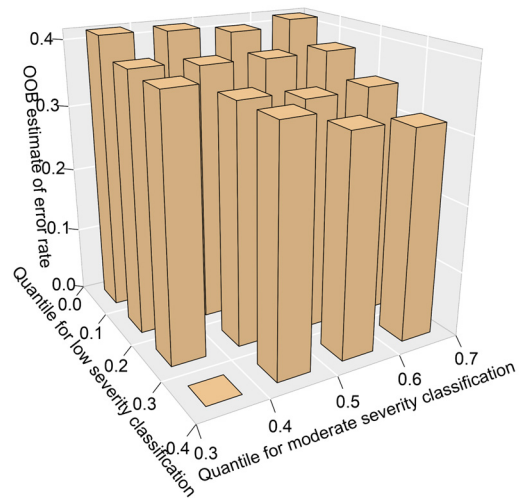
OOB estimate of error rate at 0.75 quantile for high severity classification



OOB estimate of error rate at 0.85 quantile for high severity classification



OOB estimate of error rate at 0.95 quantile for high severity classification



(a)

(b)

(c)

(d)

Figure 4. Variations of OOB estimate of error rate changes with thresholds of dNBR at the quantiles varying from 5% to 35% (low severity threshold)/35% to 65% (moderate severity threshold), when the high severity threshold are set as the dNBR values at the (a) 65%, (b) 75%, (c) 85% and (d) 95% quantiles.

259 The thresholds of dNBR for fire severity classification for different vegetation types are determined by the proposed method
 260 and the results are presented in Table 1. It is shown that the thresholds vary significantly with vegetation type. For example,
 261 for rainforests when dNBR of burnt area is around 0.20, this area should be classified as high severity. However, the burnt
 262 area with the same dNBR (0.20) would be classified as moderate severity when wildfire burns over other vegetation types.
 263 This difference is also found in the major vegetation type within different subgroups. A burn area with dNBR around 0.53 is
 264 classified as extreme high severity when fire burns over wet sclerophyll forests (grassy subformation), while this burn area is
 265 classified as high severity when fire burns over wet sclerophyll forests (shrubby subformation). The differences in
 266 classification thresholds are more significant between dry sclerophyll forests with shrub/grass subformation and shrubby
 267 subformation. The thresholds for high severity classification are 0.44 and 0.55 for burnt area over dry sclerophyll forests
 268 (shrub/grass subformation) and dry sclerophyll forests (shrubby subformation), respectively. These results indicate that using
 269 the vegetation specific thresholds would obtain more reasonable fire severity classification results, while a lot of
 270 misclassifications are found when applying fixed thresholds in fire severity classification without considering the variations in
 271 vegetation cover.

272

273 Table 1. Thresholds of dNBR for fire severity classification by vegetation type.

Vegetation	Low	Moderate	High	Extreme
Rainforests	< 0.05 (25%)	0.05 - 0.18 (25%-45%)	0.18 - 0.41 (45%-75%)	> 0.41 (75%)
Wet sclerophyll forests (Shrubby subformation)	< 0.15 (35%)	0.15 - 0.34 (35%-55%)	0.34 - 0.56 (55%-85%)	> 0.56 (85%)
Wet sclerophyll forests (Grassy subformation)	< 0.17 (35%)	0.17 - 0.34 (35%-55%)	0.34 - 0.52 (55%-85%)	> 0.52 (85%)
Grassy woodlands	< 0.15 (35%)	0.15 - 0.36 (35%-55%)	0.36 - 0.55 (55%-85%)	> 0.55 (85%)
Dry sclerophyll forests (Shrub/grass subformation)	< 0.12 (15%)	0.12 - 0.26 (15%-45%)	0.26 - 0.44 (45%-75%)	> 0.44 (75%)
Dry sclerophyll forests (Shrubby subformation)	< 0.20 (25%)	0.20 - 0.38 (25%-55%)	0.38 - 0.55 (55%-85%)	> 0.55 (85%)
Heathlands	< 0.26 (35%)	0.26 - 0.40 (35%-55%)	0.40 - 0.57 (55%-75%)	> 0.57 (75%)

274

275 4.3 Fire severity prediction results

276 The performance of vegetation specific thresholds and the importance of vegetation type are validated by the cross-validation
 277 in the RF model. Figure 5 (a) and (b) show the relative importance of variables in the RF based on samples classified by
 278 vegetation specific thresholds and fixed thresholds, respectively. The error bar represents the standard deviation (sd) of relative
 279 importance in RF models in the cross-validation experiments. The preNBR is the most influential variable with relative
 280 importance around 28% and sd around 7%. The FFDI also plays an important role in the model with relative importance and
 281 sd of 21% and 6%, respectively. The KBDI shows close relative importance to those of FFDI, the values of mean relative
 282 importance and sd are 19% and 5% respectively. While for vegetation type, the relative importance (13%) is higher than those

283 of topographic variables when the vegetation specific thresholds are applied. The sd of vegetation type is the largest (9%),
 284 owing to the differences in vegetation diversity in the training samples.

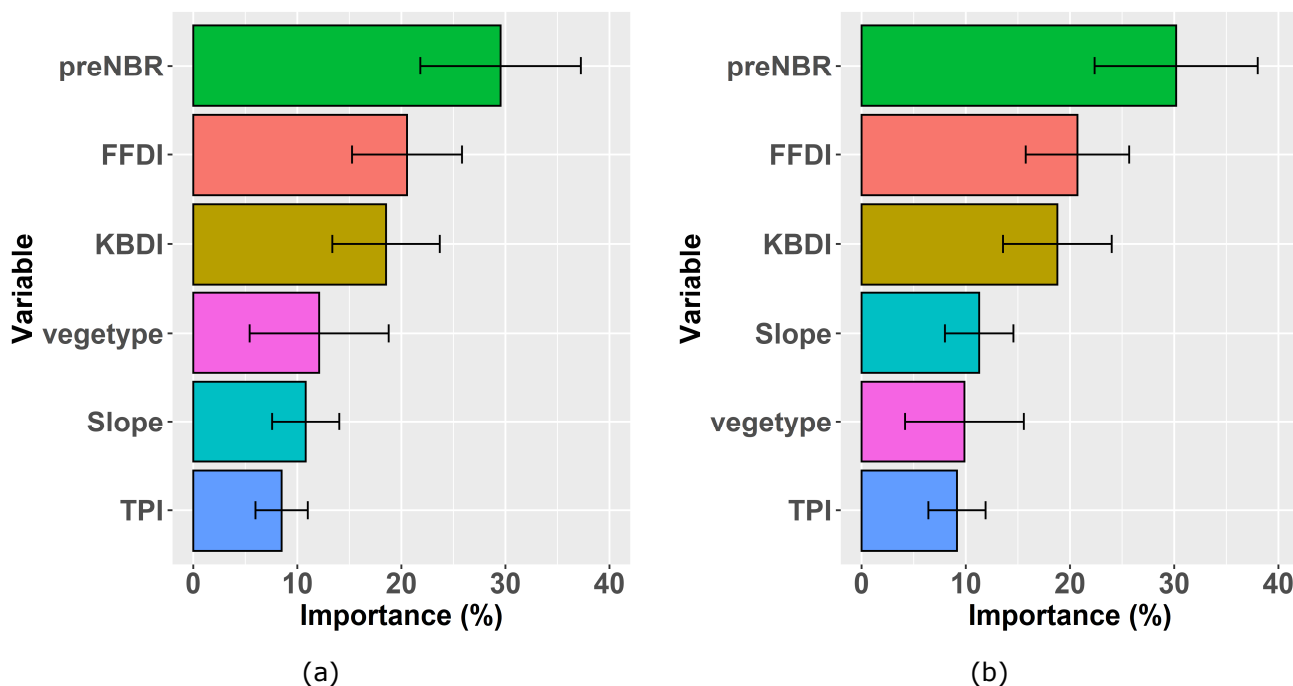


Figure 5. Relative importance of variables in RF models based on samples classified by (a) vegetation specific thresholds and (b) fixed thresholds.

285
 286 The confusion matrix of the fire severity classification results is shown in Table 2. More samples are classified into extreme
 287 high severity classification when applying vegetation specific thresholds than those using fixed thresholds. Similarly, more
 288 samples are classified into low severity while implementing fixed thresholds than vegetation specific thresholds. This indicates
 289 that using fixed thresholds without considering the vegetation type tends to underestimate the fire severity levels. While for
 290 the performance of fire severity prediction, most events of extreme high severity are correctly identified by the RF model
 291 trained by samples classified by vegetation specific thresholds while more misclassified extreme high severity and high
 292 severity events are predicted by the RF model trained by samples classified by fixed thresholds.

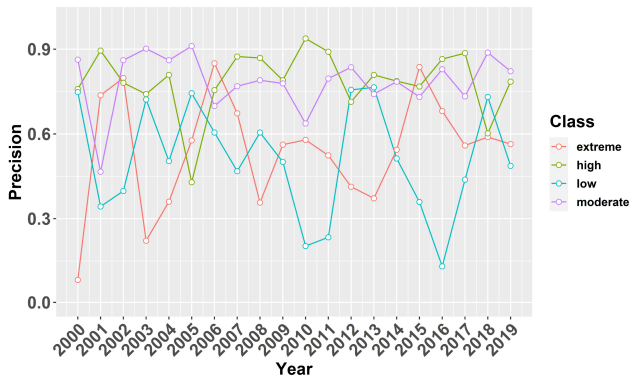
293
 294 Table 2. Confusion matrix of prediction results based on RF model trained by samples classified by vegetation specific and
 295 fixed thresholds.

	Vegetation specific				Fixed				
	Extreme	High	Moderate	Low	Extreme	High	Moderate	Low	
Extreme	52680	22782	813	9	Extreme	36573	24573	1755	30
High	4749	94899	17265	171	High	3930	64740	21498	471

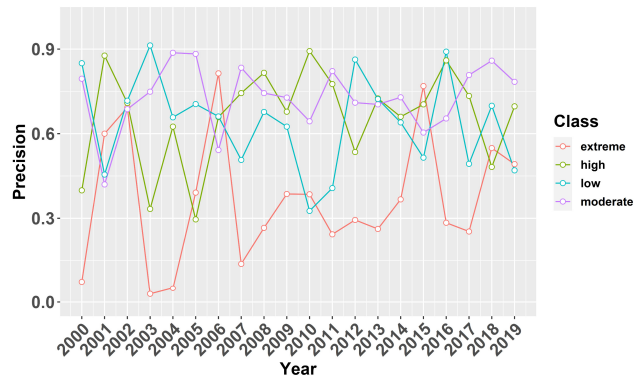
Moderate	501	20487	103536	3948	Moderate	852	19794	94857	8739
Low	147	1422	22239	36897	Low	357	2754	31299	70347

296

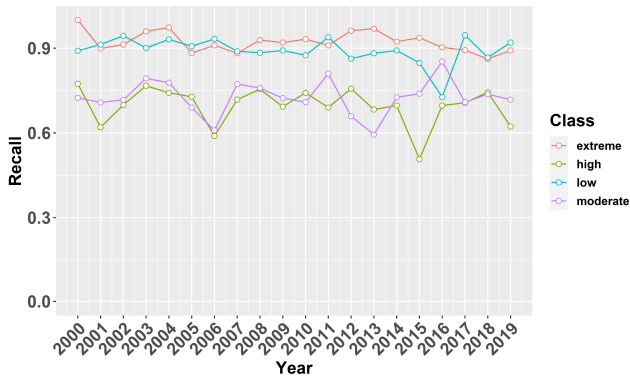
297 The overall classification accuracy calculated by equation (4) is 0.75 and 0.69, for RF models trained by samples classified by
 298 vegetation specific and fixed thresholds, respectively. Figure 6 (a), (b) and (c) show the Precision, Recall and F1 score of event
 299 severity classification results for each class label calculated by equations (5) – (7). The Accuracy, Precision, Recall results and
 300 F1 Score close to 1 indicate accurate classification results. For the classification metrics of each class label, the high severity
 301 events class exhibit the best Precision (0.85) relative to the moderate (0.76) and extreme high severity event classes (0.68),
 302 while the Recall and F1 score for high severity events class are 0.64 and 0.73, respectively. The extreme high severity events
 303 class exhibit the best Recall (0.89) relative to the other two classes, and the Precision and F1 score are 0.68 and 0.77,
 304 respectively. The performances of fire severity classification are worse for the RF model trained by samples classified by the
 305 fixed thresholds, with lower precision, recall and F1 score.



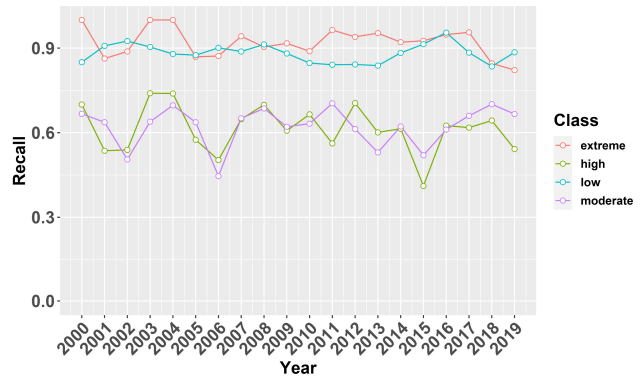
(a)



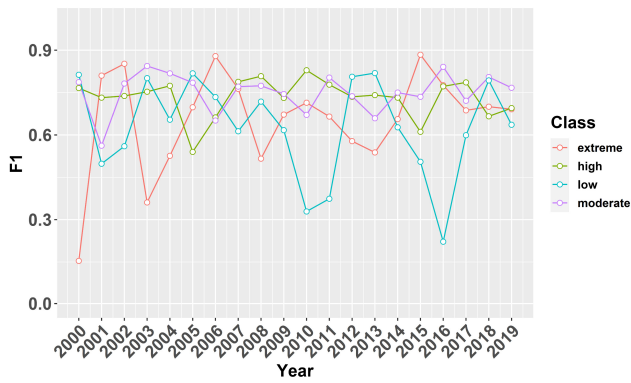
(b)



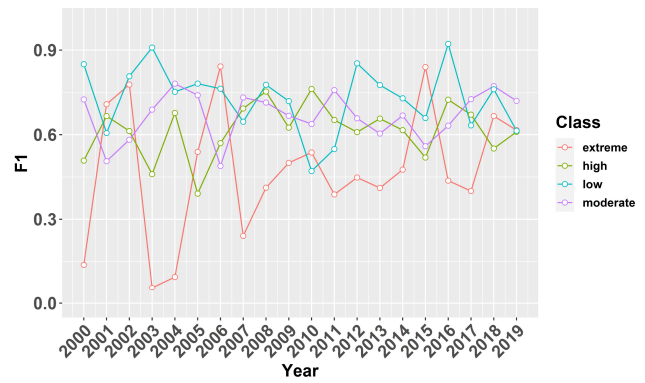
(c)



(d)



(e)



(f)

Figure 6. Results of Precision for predictions based on (a) vegetation specific thresholds and (b) fixed thresholds; The results of Recall for predictions based on (c) vegetation specific thresholds and (d) fixed thresholds; The results of F1 score for predictions based on (e) vegetation specific thresholds and (f) fixed thresholds;

306

307

308 Figure 7 displays the fire severity maps for the 2016, 2017, 2018 and 2019 wildfires in NSW from FESM, along with fire
 309 severity predictions based on vegetation specific and fixed thresholds. For the wildfire in 2016, predictions based on vegetation
 310 specific thresholds show similar spatial patterns of fire severity to those from FESM, while predictions based on fixed
 311 thresholds significantly underestimate the fire severity in the high and extreme fire severity areas of the FSEM. Similarly for
 312 the wildfire in 2018, predictions based on fixed thresholds significantly underestimate high and extreme severity compared to
 313 the FESM map, while predictions based on vegetation specific thresholds slightly underestimate extreme severity. For the
 314 wildfire in 2017, both the FESM and predictions display similar spatial distributions of fire severity level with predictions
 315 based on fixed thresholds presenting more low severity compared to FESM map. For the wildfire in 2019, however, predictions
 316 based on fixed thresholds tend to overestimate the fire severity as extreme in regions found to be high severity in FESM map,
 317 while predictions based on vegetation specific thresholds agreed better with FESM map.

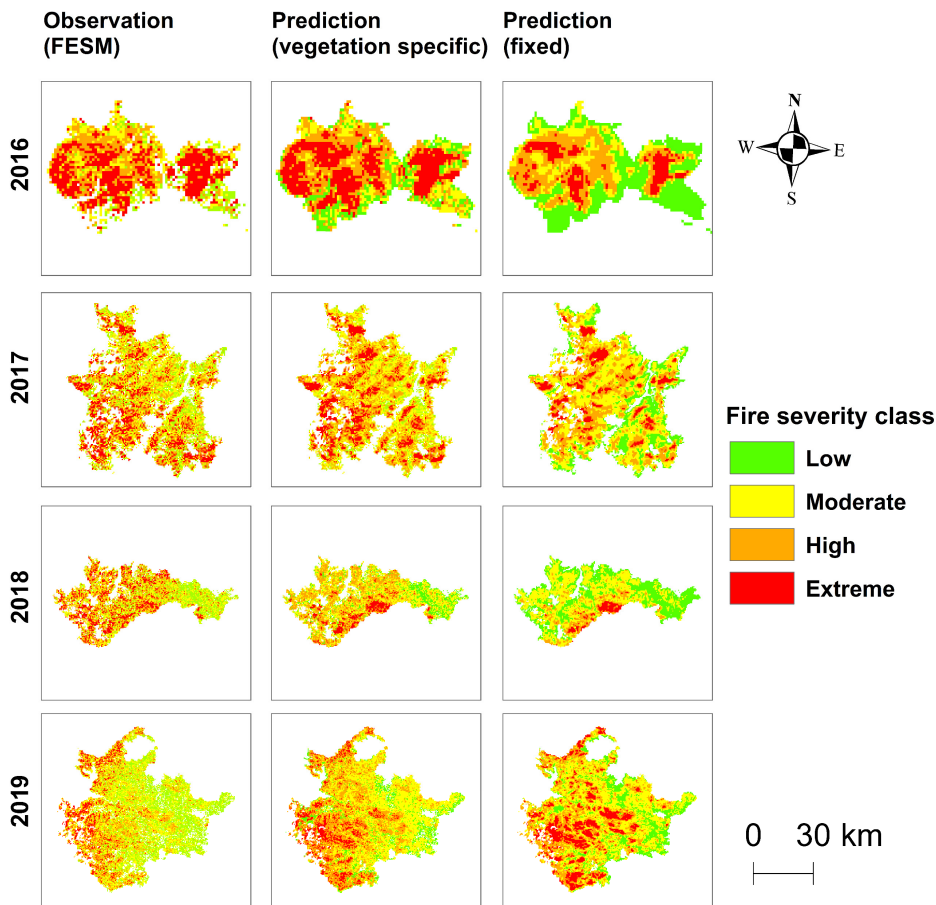


Figure 7. Fire severity classification maps from FESM and predictions based on vegetation specific and fixed thresholds for wildfires in 2016 to 2019 in NSW.

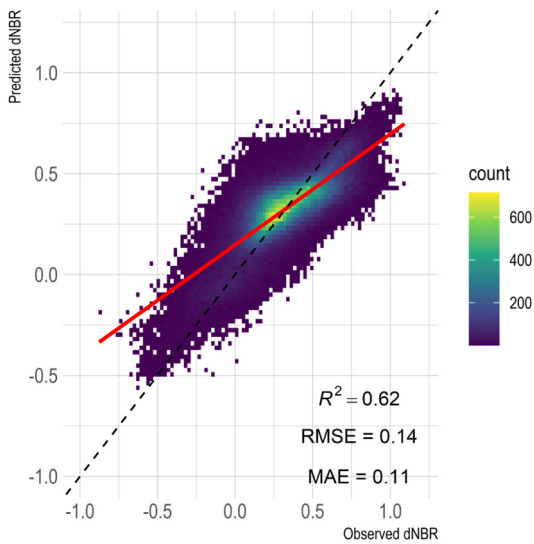
318

319 Table 3 shows the confusion matrix for fire severity classification between FESM and predictions based on vegetation specific
 320 and fixed thresholds. It is noted that predictions based on vegetation specific thresholds exhibit better ability of classing
 321 extreme and high severity with accuracy of 0.64 and 0.76, respectively. While the classification accuracy for extreme and high
 322 severity of predictions based on fixed thresholds are 0.21 and 0.39, respectively. Predictions based on vegetation specific
 323 thresholds also have better accuracy of classifying moderate severity with value of 0.62, compared to those based on fixed
 324 thresholds with value of 0.47. Both predictions based on vegetation specific and fixed thresholds show poor performance in
 325 classifying low severity, with accuracy of 0.24 and 0.26 respectively. The overall classification accuracy for predictions based
 326 on vegetation specific thresholds is 0.57, which is better than predictions based on fixed specific thresholds with accuracy of
 327 0.36.

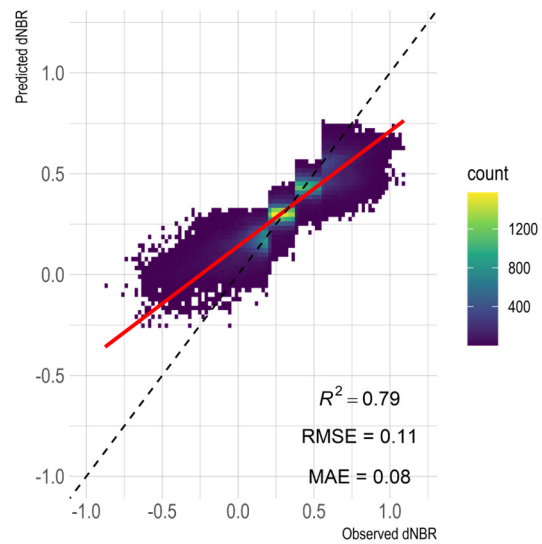
328 Table 3. Confusion matrix for fire severity classification between FESM and predictions based on vegetation specific and fixed
 329 thresholds.

	Vegetation specific				Fixed				
	Extreme	High	Moderate	Low	Extreme	High	Moderate	Low	
Extreme	4345	2378	6	3	Extreme	1448	2822	2027	435
High	1490	6947	605	1	High	1430	3561	3358	694
Moderate	3	5702	9338	5	Moderate	998	4633	7084	2333
Low	0	172	7125	2372	Low	161	1722	5264	2522

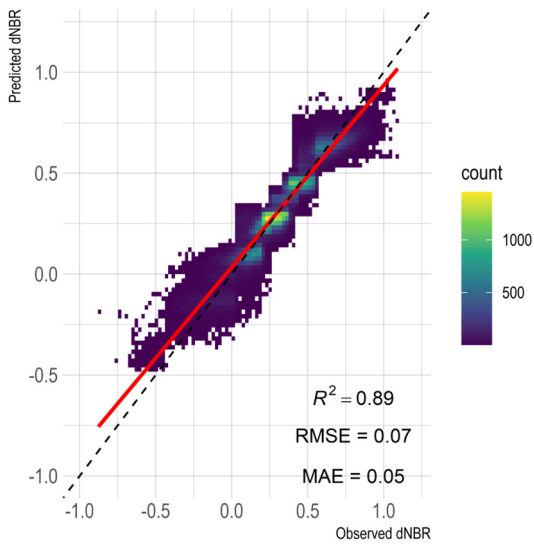
330 To evaluate the model’s performance in fire severity prediction, we apply the leave-one-year-out cross-validation method. We
 331 validate the fire severity predictions against the observed burn severity derived from Landsat images and compare the
 332 predictions based on the RF model with (and without) severity classification method. Figures 8 (a), (b) and (c) display the
 333 scatterplots of fire severity prediction against fire severity observations based on RF model without severity classification,
 334 with severity classification using the fixed threshold and using the vegetation-specific threshold, respectively. Arguably, the
 335 predictions without severity classification show strong underestimation of high fire severity events and overestimation of low
 336 burn severity events, with R^2 value of 0.62, RMSE and MAE are 0.14 and 0.11, respectively. The distributions of predictions
 337 with severity classification using the fixed threshold do not agree well with observations, though showing higher R^2 (0.79),
 338 lower RMSE and MAE values of 0.11 and 0.08, respectively. Predictions with severity classification using the vegetation-
 339 specific threshold exhibit better fire severity prediction results for high-, moderate- and low-severity events with improved R^2 ,
 340 RMSE and MAE, which are 0.89, 0.07 and 0.05, respectively.



(a)



(b)

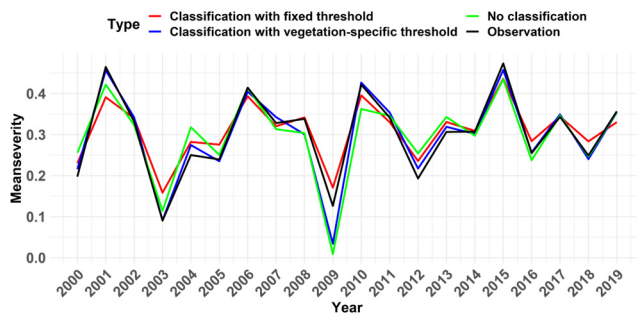


(c)

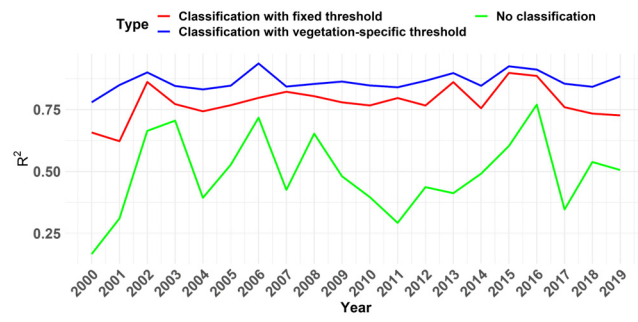
Figure 8. Scatterplots of fire severity prediction against observations based on XGBoost model (a) without severity classification; (b) with severity classification using the fixed threshold; and (c) with severity classification using the vegetation-specific threshold.

341

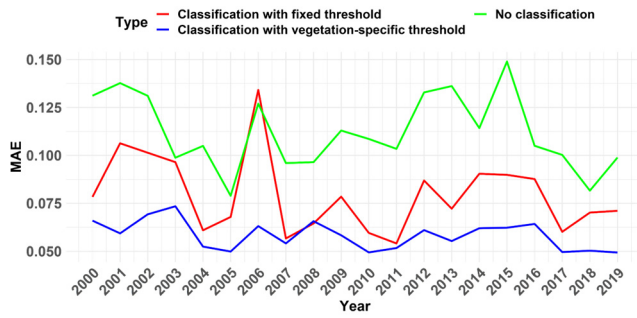
342 We also evaluate the model's ability of capturing the fire severity dynamics and magnitude in terms of mean fire severity for
 343 the selected wildfires. Figure 9 (a) displays the dynamics of predicted fire severity based on RF model with and without severity
 344 classification, while Figures 9 (b), (c) and (d) show the dynamics of associated performances of R^2 , RMSE and MAE,
 345 respectively. The predictions without severity classification are unable to capture the dynamics of mean fire severity, having
 346 the lowest R^2 and highest RMSE and MAE values. While the dynamics of the predicted fire severity with severity classification
 347 has better correlation with the observed ones compared to those without severity classification, especially the results with
 348 severity classification using the vegetation-specific threshold, which exhibit the best performance of predicting fire severity
 349 magnitude with the largest R^2 and lowest RMSE and MAE values. These results indicate that severity classification is an
 350 important process to improve the performance of fire severity prediction models.



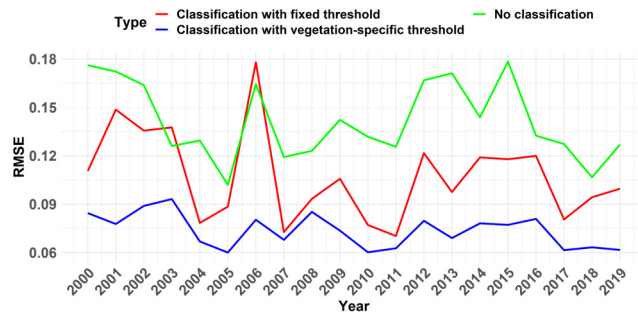
(a)



(b)



(c)



(d)

Figure 9. Time series of (a) mean fire severity, (b) R^2 , (b) RMSE and (c) MAE from 2000 to 2019 based on XGBoost models without severity classification and with severity classification using the fixed and vegetation-specific threshold.

351

352 Figure 10 depicts a summary plot of estimated SHAP values coloured by the feature values, ranked from top to bottom by their
 353 importance. It is shown that preNBR is the most important feature in the model, followed by FFDI. The KBDI is also crucial
 354 in the model. The topographic factors are also contributing to the model. We can find that having a high preNBR is associated
 355 with high and positive values on the model output, indicating the larger preNBR is the prerequisite of more severe wildfire.
 356 Similar to the effect of preNBR on the model output, a high FFDI is always associated with high and positive SHAP values,
 357 which means the more severe fire weather could lead to more destructive wildfires. Though some high KBDI is found to be
 358 associated with negative SHAP values, the KBDI still shows strong positive effect on the model output, reflecting the fact that
 359 the dry condition could favour the fire behaviour. Regarding the topography, the large slope and TPI tend to have positive
 360 SHAP values, meaning the more severe fire tends to occur in steeper and higher position.

361

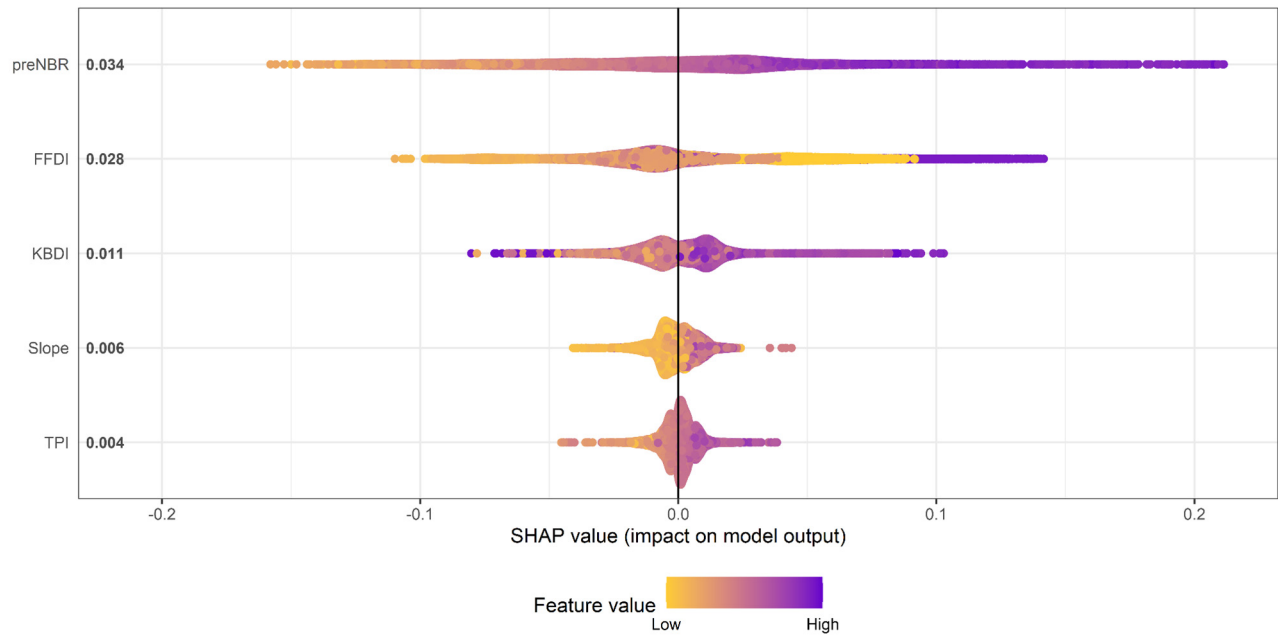


Figure 10. The SHAP values for variables predicting fire severity based on XGBoost model.

362

363 Fig. 11 displays the partial dependence plot (PDP) for each feature in the model. From Figure 11, it can be shown that the
 364 preNBR has a strong positive association with the dNBR, implying that dNBR increases with the preNBR rapidly. The FFDI
 365 shows a non-monotonic relationship with dNBR, with a decreasing trend observed when it is less than 30, a steady increasing
 366 trend between 30 to 65 and significant increasing after it exceeds 65, suggesting that the fire weather dependence is more
 367 complex. The weak correlation between KBDI and dNBR, within the range of KBDI lower than 400, indicates that KBDI has
 368 nearly no influence when it is below 400. While the positive correlation between KBDI and dNBR, within the range of 400 to
 369 600, suggest that the dry condition would intensify the fire severity. However, a declining trend of KBDI is found when it
 370 exceeds 600, meaning the impact of KBDI on dNBR becomes weaker. Regarding the slope, a negative association with dNBR
 371 is observed when it is below 3, while a positive relationship is found when it exceeds 3. The TPI shows an overall positive
 372 association with dNBR. These findings demonstrate that fire severity tends to be higher on steeper slopes and in hilltops.

373

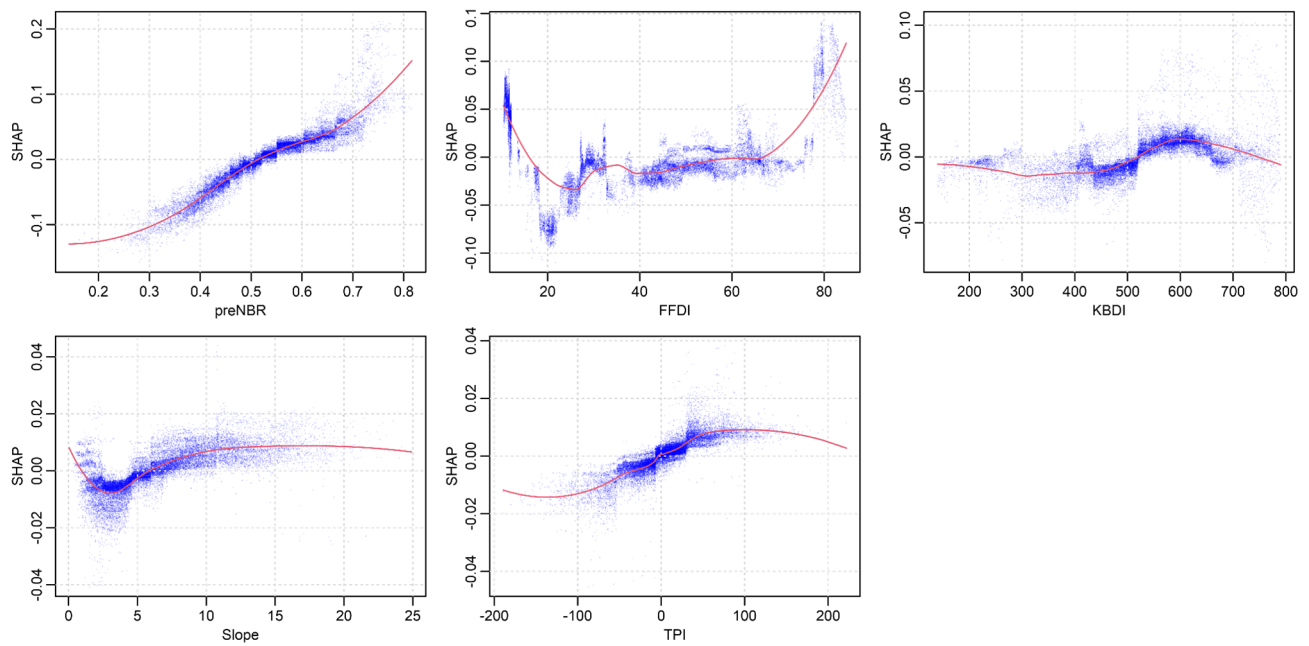


Figure 11. The variation of SHAP values as variables change.

374 5 Discussion

375 This study shows that the proposed predictive technique is capable of providing robust fire severity prediction information,
 376 which can be used for forecasting seasonal fire severity and, subsequently, impacts on biodiversity and ecosystems under
 377 future projected climate conditions.

378 We find that the RF is effective in classifying fire events into different levels of fire severity and XGBoost is a useful method
 379 to characterise the relationships between fire severity and explanatory variables (e.g., preNBR, FFDI, KBDI, slope and TPI).
 380 Fire severity is a complex function of explanatory variables gradients and these relationships may vary in different vegetation
 381 type and severity levels. The preNBR, an approximation of the pre-fire vegetation condition, plays an important role in
 382 classification and prediction, as the change in NBR pre- and post-fire, i.e. dNBR, will be dependent on both the condition of
 383 the vegetation before the fire and the degree of change to vegetation after the fire. The preNBR, indicating the pre-fire
 384 vegetation condition, might be related to the pre-fire drought. For example, drought reduces the water content of foliage (Choat
 385 et al. 2018), thus reducing preNBR, so the maximum absolute change in NBR (dNBR) possible might be smaller during a
 386 drought year than a non-drought year. The FFDI is found to be important in fire severity classification and prediction. The
 387 meteorological conditions are proven to be the most influential predictors in determining the magnitude of fire severity (Clarke
 388 et al., 2014; Bowman et al., 2021). The FFDI is the index of fire weather severity during the fire season thus is workable in
 389 determining the potential burn severity level. KBDI is another important variable in fire severity classification. It is known

390 that drought can create conditions that favour severe fires (Abram et al. 2021) and that the combined effects of fire and drought
391 can contribute to plant population declines (Gallagher et al. 2022; Nolan et al. 2021) and ecosystem transformation (Keith et
392 al. 2022). Severe drought conditions also directly contribute to forest flammability (Nolan et al. 2020). More importantly, the
393 frequency, intensity and duration of drought conditions are projected to shift under future climates (Ukkola et al. 2020). These
394 changes in drought regimes will likely be associated with increases in the size, frequency and severity of fires (Abram et al.
395 2021). TPI and slope, as important topographic factors, also have considerable influence on low fire severity. For example,
396 Bradstock et al. (2010) found burn severity is lower in valleys, probably due to effects of wind protection and higher fuel
397 moisture in moderating fire behaviour. Barker et al. (2018) found that the probability of low severity increased with slope. In
398 this study, we find that fire severity tends to be higher on steeper slopes and higher position, this might be that steep slopes
399 can intensify fire behaviour by creating a chimney effect that draws in air and accelerates the fire (Andrews and Bradshaw,
400 2012; Jolly et al., 2015; Seginer and Brandl, 2007.). Besides, higher elevations generally have lower air pressure and reduced
401 humidity, which helps fire burn more intensely (Abatzoglou and Kolden, 2011; Holden et al., 2018). Additionally, vegetation
402 on steep slopes can be thicker and more continuous, providing more fuel for the fire (Collins et al., 2009; Pausas and Fernández-
403 Muñoz, 2012).

404 One limitation of this study is that it does not consider the vegetation vertical structure parameters in the fire severity model,
405 which have been shown to influence fire behavior. Agee (1996) showed that manipulating forest structure can help to reduce
406 the severity of fire events, e.g., by reducing the crown bulk density the high severity fire would be effectively limited. Fang et
407 al. (2015) evaluated the influences and relative importance of fire weather, topography, and vegetation structure on fire size
408 and fire severity, which showed fire weather was the dominant driving factor for fire size, while vegetation structure exerted
409 stronger influences on fire severity. The study by Fernández-Guisuraga et al. (2021) indicated that severe ecosystem damage
410 was mainly driven by vegetation structure rather than topography, for example high canopy density was the main driver of
411 high burn severity. Detailed and accurate vegetation structure data require extensive field inventory and thus are mostly
412 regionally restricted. With the development of Global Ecosystem Dynamics Investigation (GEDI) project, it is possible to
413 derive reliable forest vertical structure parameters from satellite with relatively high spatial resolution and global coverage
414 (Dubayah et al., 2020). An extension of this study should incorporate data from GEDI into the fire severity model, which
415 would represent an advancement in understanding and predicting the impact of wildfires. Besides, topographic data derived
416 from SRTM presents its limits, especially in vegetated areas and terrains with pronounced slopes or certain aspects
417 [Gorokhovich and Voustianiouk, 2006; Shortridge and Messina, 2011]. The advances in DEM technology, as evidenced by
418 the improvements in the SRTM data, such as SRTM-derived 1 Second -and 3 seconds- Digital Elevation Models Version 1.0
419 for Australia, and the introduction of global COPDEM30 and TanDEM-X data [Hawker et al., 2022], offer opportunities for
420 refining fire-topography relationship analyses and potentially providing more precise fire severity prediction results. The
421 introduction of vegetation specific thresholds is proven to be beneficial for fire severity classification. The range of dNBR
422 varies significantly with vegetation types, and thus applying a fixed threshold in dNBR would lead to a large amount of
423 misclassification in fire severity levels. This kind of misclassification error is mitigated by using vegetation specific thresholds

424 in dNBR. The vegetation type also plays an important role in the RF model. The relative influence of vegetation type is larger
425 than the topographic factors while the deviation of vegetation type is the largest in the meantime. The relative influence of
426 vegetation type and the deviation changes with the number of vegetation types and its fractions in the fire event. For example,
427 five vegetation types were affected in the 2002 wildfire, and the fractions of vegetation types are: dry sclerophyll forests
428 (shrubby subformation) (30%), grassy woodlands (31 %), wet sclerophyll forests (grassy subformation) (23%), dry sclerophyll
429 forests (Shrub/grass subformation) (14%) and grasslands (2%). While in the 2019 wildfire, seven vegetation types were
430 affected, dry sclerophyll forests (shrubby subformation) accounts for 92% of the burn area. The relative influence of vegetation
431 type in the 2002 wildfire is around 10% while only 5% in the 2019 wildfire. This could also explain why no significant
432 differences are found between fire severity maps using vegetation specific thresholds and fixed thresholds in the 2019 wildfire.
433 Since more than 90% of the burn area in the 2019 wildfire is covered by dry sclerophyll forests (shrubby subformation) and
434 the fixed thresholds are adopted from the thresholds of dry sclerophyll forests (shrubby subformation), the fire severity
435 classification for 2019 wildfire is almost equal to the fire severity classification for dry sclerophyll forests (shrubby
436 subformation).

437 This study develops a predictive technique which is capable of providing robust fire severity classification and prediction
438 information for historical events, which also has the potential to forecast the seasonal fire severity. The input variables to the
439 model could be obtained from other forecast models: fire weather related variables can be extracted from the Weather Research
440 and Forecasting (WRF) model. The NBR images are derived from the Landsat 5,7 and 8 in this study, while it is also applicable
441 to other image sources based on the reflectance information from NIR and SWIR, such as the new launched Landsat 9 and
442 Sentinel-2 (Mallinis et al., 2018; Howe et al. 2022). Owing to the seasonality characteristic of preNBR, we can infer the
443 preNBR in the fire season based on the historical preNBR time series derived from the image sources. The vegetation type and
444 topographic factors are static variables, while the variables for calculating FFDI and KBDI, e.g., wind speed, relative humidity,
445 precipitation, air temperature, are available from WRF outputs. Quick assessment of fire severity for wildfires are accessible
446 based on the proposed predictive technique, once the burn area are derived from the burn area prediction models (Alkhatib,
447 2014; Castelli et al., 2015) or monitoring products (e.g., MODIS Burned Area Product, MCD64A1).

448 With the rapid development of new technologies such as LiDAR and Unmanned Aerial Vehicle (UAV), integration of data
449 from these platforms can represent a promising avenue to enhance our understanding and management of wildfires. LiDAR
450 technology, with its capability to produce high-resolution vegetation structural and topography information could facilitate the
451 accurate modelling of fire severity (Hudak et al., 2012; Hébert et al., 2017). On the other hand, the agility and precision of
452 UAVs in data collection enable real-time monitoring of fire spreading, which significantly enhances our ability to map burn
453 areas in real-time (Véga et al., 2018; Zheng et al., 2019).

454 6 Conclusions

455 This study introduces the vegetation specific thresholds in fire severity classification for wildfires over NSW, Australia. We
456 use the pre-fire season drought conditions, topography, and the fire season meteorological conditions as input to build the
457 predictive model and the performances are validated by EXtreme Gradient Boosting (XGBoost) to predict the fire severity,
458 proxied by dNBR.

459 Using the vegetation specific thresholds we could improve the classification accuracy in fire severity levels. Specifically,
460 compared with the fire severity classifications from FESM over NSW, we found fire severity classification results using
461 vegetation specific thresholds show good agreement to those from FESM, with accuracy of 0.64 and 0.76 in extreme and high
462 severity classification. Using a leave-one-out cross-validation, the severity classification results showed an improved
463 classification accuracy of 0.75 based on the proposed vegetation specific thresholds, compared to those based on fixed
464 thresholds (0.69). The predictive performance of XGBoost model is improved as well based on the classification results, with
465 determination coefficient (R^2), mean absolute error (MPE) and root mean square error (RMSE) values of 0.89, 0.05, and 0.07,
466 respectively. We show that the preNBR is the most important variable in fire severity classification and prediction, followed
467 by FFDI and KBDI. The PDP of FFDI and KBDI indicate that the likelihood of high severity increases when weather and
468 drought conditions become more severe. From the responses of dNBR to topographic factors, the probability of high severity
469 increases with slope and elevation. The role of vegetation type in fire severity prediction becomes more important for large
470 fires where more diverse vegetation is affected.

471 The results demonstrate that the prediction technique performs well predicting fire severity of historic fires (2000-2019) in the
472 Australian state of NSW, while it also shows the potential to be applicable for seasonal fire severity forecasts, owing to the
473 availability of the predictor variables in seasonal forecasting outputs. With the expected increase in wind speed, temperature
474 and drought conditions exhibited in future climate projections, this prediction technique can also be used to evaluate the
475 variation of fire severity under climate change. Future challenges of this study include incorporating different variables, such
476 as refined topography as well as weather and vegetation structure, from various data source to improve the accuracy of fire
477 severity prediction and scaling up the application of the developed model globally. In addition, the sensitivity analysis of the
478 selected time window to define the fire event and obtain the associated weather conditions is promoted to improve our
479 understanding of the relationship between weather conditions and fire occurrences. By adjusting the time window and possibly
480 integrating more precise burn date data, we can work towards a more accurate and physically meaningful analysis of fire events
481 and their contributing factors.

482

483 **Author contributions:** Kang He: Data curation, Visualization, Writing-Original draft preparation. Xinyi Shen: Supervision,
484 Methodology, Writing- Reviewing and Editing. Emmanouil N. Anagnostou: Supervision, Methodology, Writing-Reviewing
485 and Editing Cory Merow: Methodology, Writing-Reviewing and Editing. Efthymios Nikolopoulos: Data curation, Writing-

486 Reviewing and Editing. Rachael Gallagher: Data curation, Writing-Reviewing and Editing Feifei Yang: Methodology,
487 Writing- Reviewing and Editing.

488

489 **Competing interests:** The contact author has declared that none of the authors has any competing interests.
490

491 **Acknowledgements:** This research was supported by National Science Foundation HDR award entitled “Collaborative
492 Research: Near term forecast of Global Plant Distribution Community Structure, and Ecosystem Function”. Kang He received
493 the support of China Scholarship Council for four years' Ph.D. study in University of Connecticut (under grant agreement no.
494 201906320068).
495

496 **References**

- 497 Agee, James K. (1996). "The influence of forest structure on fire behavior." In Proceedings of the 17th annual forest vegetation
498 management conference, pp. 52-68.
- 499 Fang, L., Yang, J., Zu, J., Li, G. and Zhang, J., (2015). Quantifying influences and relative importance of fire weather,
500 topography, and vegetation on fire size and fire severity in a Chinese boreal forest landscape. *Forest Ecology and Management*,
501 356, pp.2-12.
- 502 Fernández-Guisuraga, J.M., Suárez-Seoane, S., García-Llamas, P. and Calvo, L., (2021). Vegetation structure parameters
503 determine high burn severity likelihood in different ecosystem types: A case study in a burned Mediterranean landscape.
504 *Journal of environmental management*, 288, p.112462.
- 505 Dubayah, R., Blair, J.B., Goetz, S., Fatoyinbo, L., Hansen, M., Healey, S., Hofton, M., Hurtt, G., Kellner, J., Luthcke, S. and
506 Armston, J., 2020. The Global Ecosystem Dynamics Investigation: High-resolution laser ranging of the Earth's forests and
507 topography. *Science of remote sensing*, 1, p.100002.
- 508 Hudak, A. T., Strand, E. K., Vierling, L. A., Byrne, J. C., Eitel, J. U., & Martinuzzi, S. 2012. Quantifying aboveground forest
509 carbon pools and fluxes from repeat LiDAR surveys. *Remote Sensing of Environment*, 123, 25-40.
- 510 Hébert, F., & Mallet, C. 2017. Forest fire severity assessment using LiDAR in a Mediterranean environment. *Remote Sensing*,
511 9(9), 908.
- 512 Véga, C., Martín, M. P., López, F. J., García, A. M., & Pérez, J. A. (2018). Fire spread and vegetation monitoring by using a
513 UAV system. *Drones*, 2(4), 31.
- 514 Zheng, D., Jiang, Y., & Cheng, T. (2019). UAV-based remote sensing technology in the rapid monitoring of forest fires.
515 *International Journal of Remote Sensing*, 40(11), 4257-4275.
- 516 Abatzoglou, J. T., Williams, A. P., & Barbero, R. (2019). Global emergence of anthropogenic climate change in fire weather
517 indices. *Geophysical Research Letters*, 46(1), 326-336.

518 Abatzoglou, J.T. and Kolden, C.A., 2011. Climate change in western US deserts: potential for increased wildfire and invasive
519 annual grasses. *Rangeland Ecology & Management*, 64(5), pp.471-478.

520 Abram, N. J., Henley, B. J., Sen Gupta, A., Lippmann, T. J., Clarke, H., Dowdy, A. J., ... & Boer, M. M. (2021). Connections
521 of climate change and variability to large and extreme forest fires in southeast Australia. *Communications Earth &
522 Environment*, 2(1), 1-17.

523 Alkhatib, A.A., 2014. A review on forest fire detection techniques. *International Journal of Distributed Sensor Networks*, 10(3),
524 p.597368.

525 Andrews, P. L., & Bradshaw, L. S. (2012). The effects of slope and aspect on fire behavior. In *Fire in California's ecosystems*
526 (pp. 153-171). University of California Press. <https://doi.org/10.1525/california/9780520278806.003.0011>

527 Archibald, S., Lehmann, C. E., Gómez-Dans, J. L., & Bradstock, R. A. (2013). Defining pyromes and global syndromes of
528 fire regimes. *Proceedings of the National Academy of Sciences*, 110(16), 6442-6447.

529 Barker, J. W., & Price, O. F. (2018). Positive severity feedback between consecutive fires in dry eucalypt forests of southern
530 Australia. *Ecosphere*, 9(3), e02110.

531 Boby, L. A., Schuur, E. A., Mack, M. C., Verbyla, D., & Johnstone, J. F. (2010). Quantifying fire severity, carbon, and nitrogen
532 emissions in Alaska's boreal forest. *Ecological Applications*, 20(6), 1633-1647.

533 Bowman, D. M., Williamson, G. J., Gibson, R. K., Bradstock, R. A., & Keenan, R. J. (2021). The severity and extent of the
534 Australia 2019–20 Eucalyptus forest fires are not the legacy of forest management. *Nature Ecology & Evolution*, 5(7), 1003-
535 1010.

536 Bradstock, R. A., Hammill, K. A., Collins, L., & Price, O. (2010). Effects of weather, fuel and terrain on fire severity in
537 topographically diverse landscapes of south-eastern Australia. *Landscape Ecology*, 25(4), 607-619.

538 Breiman, L. (2001). Random forests. *Machine learning*, 45(1), 5-32.

539 Castelli, M., Vanneschi, L. and Popovič, A., 2015. Predicting burned areas of forest fires: an artificial intelligence approach.
540 *Fire ecology*, 11(1), pp.106-118.

541 Chen, T. and Guestrin, C., 2016, August. Xgboost: A scalable tree boosting system. In *Proceedings of the 22nd acm sigkdd
542 international conference on knowledge discovery and data mining* (pp. 785-794).

543 Chen, T., He, T., Benesty, M., Khotilovich, V., Tang, Y., Cho, H., Chen, K., Mitchell, R., Cano, I. and Zhou, T., 2015. Xgboost:
544 extreme gradient boosting. *R package version 0.4-2*, 1(4), pp.1-4.

545 Clarke, H., Tran, B., Boer, M. M., Price, O., Kenny, B., & Bradstock, R. (2019). Climate change effects on the frequency,
546 seasonality and interannual variability of suitable prescribed burning weather conditions in south-eastern Australia.
547 *Agricultural and Forest Meteorology*, 271, 148-157.

548 Clarke, P. J., Knox, K. J., Bradstock, R. A., Munoz-Robles, C., & Kumar, L. (2014). Vegetation, terrain and fire history shape
549 the impact of extreme weather on fire severity and ecosystem response. *Journal of Vegetation Science*, 25(4), 1033-1044.

550 Collins, B. M., Kelly, M., Van Wagendonk, J. W., & Stephens, S. L. (2007). Spatial patterns of large natural fires in Sierra
551 Nevada wilderness areas. *Landscape Ecology*, 22(4), 545-557.

552 Collins, B. M., Miller, J. D., Thode, A. E., Kelly, M., & van Wagtenonk, J. W. (2009). Interactions among wildland fires in
553 a long-established Sierra Nevada natural fire area. *Ecosystems*, 12(1), 114-128. <https://doi.org/10.1007/s10021-008-9211-1>

554 Collins, L., Bennett, A. F., Leonard, S. W., & Penman, T. D. (2019). Wildfire refugia in forests: Severe fire weather and
555 drought mute the influence of topography and fuel age. *Global Change Biology*, 25(11), 3829-3843.

556 Collins, L., Bradstock, R. A., & Penman, T. D. (2013). Can precipitation influence landscape controls on wildfire severity? A
557 case study within temperate eucalypt forests of south-eastern Australia. *International Journal of Wildland Fire*, 23(1), 9-20.

558 Dillon, G. K., Holden, Z. A., Morgan, P., Crimmins, M. A., Heyerdahl, E. K., & Luce, C. H. (2011). Both topography and
559 climate affected forest and woodland burn severity in two regions of the western US, 1984 to 2006. *Ecosphere*, 2(12), 1-33.

560 Dowdy, A. J., Mills, G. A., Finkele, K., & De Groot, W. (2009). Australian fire weather as represented by the McArthur forest
561 fire danger index and the Canadian forest fire weather index (p. 91). Melbourne: Centre for Australian Weather and Climate
562 Research.

563 Eidenshink, J., Schwind, B., Brewer, K., Zhu, Z.L., Quayle, B. and Howard, S., 2007. A project for monitoring trends in burn
564 severity. *Fire ecology*, 3(1), pp.3-21.

565 Fang, L., Yang, J., White, M., & Liu, Z. (2018). Predicting potential fire severity using vegetation, topography and surface
566 moisture availability in a Eurasian boreal forest landscape. *Forests*, 9(3), 130.

567 Gallagher, R. V., Allen, S. P., Mackenzie, B. D., Keith, D. A., Nolan, R. H., Rumpff, L., ... & Auld, T. D. (2022). An integrated
568 approach to assessing abiotic and biotic threats to post-fire plant species recovery: Lessons from the 2019–2020 Australian
569 fire season. *Global Ecology and Biogeography*.

570 Gallagher, R. V., Allen, S., Mackenzie, B. D., Yates, C. J., Gosper, C. R., Keith, D. A., ... & Auld, T. D. (2021). High fire
571 frequency and the impact of the 2019–2020 megafires on Australian plant diversity. *Diversity and Distributions*, 27(7), 1166-
572 1179.

573 García, M. L., & Caselles, V. (1991). Mapping burns and natural reforestation using Thematic Mapper data. *Geocarto*
574 *International*, 6(1), 31-37.

575 Hammill, K. A., & Bradstock, R. A. (2006). Remote sensing of fire severity in the Blue Mountains: influence of vegetation
576 type and inferring fire intensity. *International Journal of Wildland Fire*, 15(2), 213-226.

577 Harris, L., & Taylor, A. H. (2015). Topography, fuels, and fire exclusion drive fire severity of the Rim Fire in an old-growth
578 mixed-conifer forest, Yosemite National Park, USA. *Ecosystems*, 18(7), 1192-1208.

579 Harris, L., & Taylor, A. H. (2017). Previous burns and topography limit and reinforce fire severity in a large wildfire.
580 *Ecosphere*, 8(11), e02019.

581 Hennessy, K., Lucas, C., Nicholls, N., Bathols, J., Suppiah, R., & Ricketts, J. (2005). Climate change impacts on fire-weather
582 in south-east Australia. Climate Impacts Group, CSIRO Atmospheric Research and the Australian Government Bureau of
583 Meteorology, Aspendale.

584 Holden, Z. A., Morgan, P., & Evans, J. S. (2009). A predictive model of burn severity based on 20-year satellite-inferred burn
585 severity data in a large southwestern US wilderness area. *Forest Ecology and Management*, 258(11), 2399-2406.

586 Holden, Z.A., Swanson, A., Luce, C.H., Jolly, W.M., Maneta, M., Oyler, J.W., Warren, D.A., Parsons, R. and Affleck, D.,
587 2018. Decreasing fire season precipitation increased recent western US forest wildfire activity. *Proceedings of the National*
588 *Academy of Sciences*, 115(36), pp.E8349-E8357.

589 Hudak, A. T., Ottmar, R. D., Vihnanek, R. E., Brewer, N. W., Smith, A. M., & Morgan, P. (2013). The relationship of post-
590 fire white ash cover to surface fuel consumption. *International Journal of Wildland Fire*, 22(6), 780-785.

591 Jolly, W. M., Cochrane, M. A., Freeborn, P. H., Holden, Z. A., Brown, T. J., Williamson, G. J., & Bowman, D. M. J. S. (2015).
592 Climate-induced variations in global wildfire danger from 1979 to 2013. *Nature Communications*, 6, 7537.
593 <https://doi.org/10.1038/ncomms8537>

594 Keeley, J. E. (2009). Fire intensity, fire severity and burn severity: a brief review and suggested usage. *International journal*
595 *of wildland fire*, 18(1), 116-126.

596 Keetch, J. J., & Byram, G. M. (1968). A drought index for forest fire control. USDA Forest Service Research Paper SE-38.
597 Asheville, NC.

598 Keith, D. A. (2004). Ocean shores to desert dunes: the native vegetation of New South Wales and the ACT. Department of
599 Environment and Conservation (NSW).

600 Keith, D. A., Allen, S. P., Gallagher, R. V., Mackenzie, B. D., Auld, T. D., Barrett, S., ... & Tozer, M. G. (2022). Fire-related
601 threats and transformational change in Australian ecosystems. *Global Ecology and Biogeography*.

602 Key, C.H. and Benson, N.C., 2006. Landscape assessment (LA). FIREMON: Fire effects monitoring and inventory system,
603 164, pp.LA-1.

604 Lentile, L. B., Holden, Z. A., Smith, A. M., Falkowski, M. J., Hudak, A. T., Morgan, P., ... & Benson, N. C. (2006). Remote
605 sensing techniques to assess active fire characteristics and post-fire effects. *International Journal of Wildland Fire*, 15(3), 319-
606 345.

607 Lutes, D.C., Keane, R.E., Caratti, J.F., Key, C.H., Benson, N.C., Sutherland, S. and Gangi, L.J., 2006. FIREMON: Fire effects
608 monitoring and inventory system. Gen. Tech. Rep. RMRS-GTR-164. Fort Collins, CO: US Department of Agriculture, Forest
609 Service, Rocky Mountain Research Station. 1 CD., 164.

610 McArthur AG (1967). Fire behaviour in eucalypt forests. Commonwealth of Australia, Forest and Timber Bureau Leaflet 107.
611 (Canberra, ACT, Australia)

612 Miller, J. D., Knapp, E. E., Key, C. H., Skinner, C. N., Isbell, C. J., Creasy, R. M., & Sherlock, J. W. (2009). Calibration and
613 validation of the relative differenced Normalized Burn Ratio (RdNBR) to three measures of fire severity in the Sierra Nevada
614 and Klamath Mountains, California, USA. *Remote Sensing of Environment*, 113(3), 645-656.

615 Morgan, P., Keane, R. E., Dillon, G. K., Jain, T. B., Hudak, A. T., Karau, E. C., ... & Strand, E. K. (2014). Challenges of
616 assessing fire and burn severity using field measures, remote sensing and modelling. *International Journal of Wildland Fire*,
617 23(8), 1045-1060.

618 Nolan, R. H., Boer, M. M., Collins, L., Resco de Dios, V., Clarke, H. G., Jenkins, M., ... & Bradstock, R. A. (2020). Causes
619 and consequences of eastern Australia's 2019-20 season of mega-fires. *Global change biology*.

620 Nolan, R. H., Collins, L., Leigh, A., Ooi, M. K., Curran, T. J., Fairman, T. A., ... & Bradstock, R. (2021). Limits to post-fire
621 vegetation recovery under climate change. *Plant, cell & environment*, 44(11), 3471-3489.

622 Pausas, J. G., & Fernández-Muñoz, S. (2012). Fire regime changes in the Western Mediterranean Basin: from fuel-limited to
623 drought-driven fire regime. *Climatic Change*, 110(1-2), 215-226. <https://doi.org/10.1007/s10584-011-0060-6>

624 Seginer, I., Körner, C., & Brandl, H. (2007). Topography and microclimate of exposed sites in a dry alpine valley. *Arctic,*
625 *Antarctic, and Alpine Research*, 39(3), 463-469. [https://doi.org/10.1657/1523-0430\(2007\)39\[463:TAMOES\]2.0.CO;2](https://doi.org/10.1657/1523-0430(2007)39[463:TAMOES]2.0.CO;2)

626 Shine, J. (2020). Statement regarding Australian bushfires. [https://www.science.org.au/news-and-events/news-and-media-](https://www.science.org.au/news-and-events/news-and-media-releases/australian-bushfires-why-they-are-unprecedented)
627 [releases/australian-bushfires-why-they-are-unprecedented](https://www.science.org.au/news-and-events/news-and-media-releases/australian-bushfires-why-they-are-unprecedented). Accessed 4 February 2020.

628 Soverel, N. O., Perrakis, D. D., & Coops, N. C. (2010). Estimating burn severity from Landsat dNBR and RdNBR indices
629 across western Canada. *Remote Sensing of Environment*, 114(9), 1896-1909.

630 Speer, M. S., Wiles, P., & Pepler, A. (2009). Low pressure systems off the New South Wales coast and associated hazardous
631 weather: establishment of a database. *Australian Meteorological and Oceanographic Journal*, 58(1), 29.

632 Takeuchi, W., Darmawan, S., Shofiyati, R., Khiem, M. V., Oo, K. S., Pimple, U., & Heng, S. (2015, October). Near-real time
633 meteorological drought monitoring and early warning system for croplands in asia. In *Asian Conference on Remote Sensing*
634 *2015: Fostering Resilient Growth in Asia* (Vol. 1, pp. 171-178).

635 Tran, B.N., Tanase, M.A., Bennett, L.T. and Aponte, C., 2018. Evaluation of spectral indices for assessing fire severity in
636 Australian temperate forests. *Remote sensing*, 10(11), p.1680.

637 Ukkola, A. M., De Kauwe, M. G., Roderick, M. L., Abramowitz, G., & Pitman, A. J. (2020). Robust future changes in
638 meteorological drought in CMIP6 projections despite uncertainty in precipitation. *Geophysical Research Letters*, 47(11),
639 e2020GL087820.

640 Wang, C., & Glenn, N. F. (2009). Estimation of fire severity using pre-and post-fire LiDAR data in sagebrush steppe
641 rangelands. *International Journal of Wildland Fire*, 18(7), 848-856.

642 Mallinis, G., Mitsopoulos, I. and Chrysafi, I. Evaluating and comparing Sentinel 2A and Landsat-8 Operational Land Imager
643 (OLI) spectral indices for estimating fire severity in a Mediterranean pine ecosystem of Greece. *GIsci Remote Sens*, 55(1), 1-
644 18, <https://doi.org/10.1080/15481603.2017.1354803>, 2018.

645 Howe, A.A., Parks, S.A., Harvey, B.J., Saberi, S.J., Lutz, J.A. and Yocom, L.L. Comparing Sentinel-2 and Landsat 8 for burn
646 severity mapping in Western North America. *Remote Sensing*, 14(20), 5249, <https://doi.org/10.3390/rs14205249>, 2022.

647 Collins, L., Griffioen, P., Newell, G., Mellor, A., 2018. The utility of Random Forests for wildfire severity mapping. *Remote*
648 *Sensing of Environment* 216, 374–384. <https://doi.org/10.1016/j.rse.2018.07.005>

649 Dixon, D.J., Callow, J.N., Duncan, J.M.A., Setterfield, S.A., Pauli, N., 2022. Regional-scale fire severity mapping of
650 Eucalyptus forests with the Landsat archive. *Remote Sensing of Environment* 270, 112863.
651 <https://doi.org/10.1016/j.rse.2021.112863>

652 Gorokhovich, Y., Voustianiouk, A., 2006. Accuracy assessment of the processed SRTM-based elevation data by CGIAR using
653 field data from USA and Thailand and its relation to the terrain characteristics. *Remote Sensing of Environment* 104, 409–415.
654 <https://doi.org/10.1016/j.rse.2006.05.012>

655 Hawker, L., Uhe, P., Paulo, L., Sosa, J., Savage, J., Sampson, C., Neal, J., 2022. A 30 m global map of elevation with forests
656 and buildings removed. *Environ. Res. Lett.* 17, 024016. <https://doi.org/10.1088/1748-9326/ac4d4f>

657 Shortridge, A., Messina, J., 2011. Spatial structure and landscape associations of SRTM error. *Remote Sensing of Environment*
658 115, 1576–1587. <https://doi.org/10.1016/j.rse.2011.02.017>

659 Weiss, A., 2001, July. Topographic position and landforms analysis. In Poster presentation, ESRI user conference, San Diego,
660 CA (Vol. 200).

661 Collins, L., Clarke, H., Clarke, M.F., McColl Gausden, S.C., Nolan, R.H., Penman, T. and Bradstock, R., 2022. Warmer and
662 drier conditions have increased the potential for large and severe fire seasons across south - eastern Australia. *Global Ecology*
663 *and Biogeography*, 31(10), pp.1933-1948.

664

665

666

667